A Novel Mouse Model of Acute-on-Chronic Cholestatic Alcoholic Liver Disease: A Systems Biology Comparison With Human Alcoholic Hepatitis.

Shinji Furuya, Josepmaria Argemi, Takeki Uehara, Yuuki Katou, Derrick E Fouts, Bernd Schnabl, Laurent Dubuquoy, Abha Belorkar, Rajanikanth Vadigepalli, Hiroshi Kono, et al.

▶ **To cite this version:**

Shinji Furuya, Josepmaria Argemi, Takeki Uehara, Yuuki Katou, Derrick E Fouts, et al.. A Novel Mouse Model of Acute-on-Chronic Cholestatic Alcoholic Liver Disease: A Systems Biology Comparison With Human Alcoholic Hepatitis.. Alcoholism: Clinical and Experimental Research, 2020, Alcoholism, clinical and experimental research, 44, pp.87-101. 10.1111/acer.14234 . hal-03113156

HAL Id: hal-03113156
https://hal.univ-lille.fr/hal-03113156v1

Submitted on 19 Mar 2024

HAL is a multi-disciplinary open access archive for the deposit and dissemination of scientific research documents, whether they are published or not. The documents may come from teaching and research institutions in France or abroad, or from public or private research centers.

L'archive ouverte pluridisciplinaire **HAL**, est destinée au dépôt et à la diffusion de documents scientifiques de niveau recherche, publiés ou non, émanant des établissements d'enseignement et de recherche français ou étrangers, des laboratoires publics ou privés.

Author Manuscript

Author Manuscript

Author Manuscript

Author Manuscript

HHS Public Access

Author manuscript

Alcohol Clin Exp Res. Author manuscript; available in PMC 2021 January 01.

Published in final edited form as:

Alcohol Clin Exp Res. 2020 January ; 44(1): 87–101. doi:10.1111/acer.14234.

A novel mouse model of acute-on-chronic cholestatic alcoholic liver disease: A systems biology comparison with human alcoholic hepatitis

Shinji Furuya[1], **Josepmaria Argemi**[2], **Takeki Uehara**[3], **Yuuki Katou**[3], **Derrick E. Fouts**[4], **Bernd Schnabl**[5], **Laurent Dubuquoy**[6], **Abha Belorkar**[7], **Rajanikanth Vadigepalli**[7], **Hiroshi Kono**[8], **Ramon Bataller**[3], **Ivan Rusyn**[1,*]

[1]Department of Veterinary Integrative Biosciences, Texas A&M University, College Station, TX 77843, USA

[2]Center for Liver Diseases, Pittsburgh Research Center, University of Pittsburgh Medical Center, Pittsburgh, PA 15261, USA

[3]Laboratory of Veterinary Pathology, Osaka Prefecture University, Osaka 599-8531, Japan

[4]Rockville Campus, J. Craig Venter Institute, Rockville, MD 20850, USA

[5]Department of Medicine, University of California San Diego, La Jolla, CA 92093, USA

[6]Lille Service des Maladies de l'Appareil Digestif, Hôpital Huriez, Unité INSERM 995, Faculté de médecine, 59045 Lille, France

[7]Department of Pathology, Anatomy & Cell Biology, Thomas Jefferson University, Philadelphia, PA 19107, USA

[8]First Department of Surgery, University of Yamanashi, Yamanashi Prefecture 400-8510, Japan

Abstract

Background: Alcohol-related liver disease is the main cause of liver-related mortality worldwide. The development of novel targeted therapies for patients with advanced forms (*i.e.*, alcoholic hepatitis, AH) is hampered by the lack of suitable animal models. Here, we developed a novel mouse model of acute-on-chronic alcohol liver injury with cholestasis and fibrosis and performed an extensive molecular comparative analysis with human AH.

Methods: For the mouse model of acute-on-chronic liver injury, we used 3, 5-diethoxycarbonyl-1,4-dihydrocollidine (DDC, 0.05% w/w) diet for 8 weeks to establish cholestatic liver fibrosis. After one-week washout period, male mice were fed intragastrically for 4 weeks with up to 24 g/kg of ethyl alcohol in a high-fat diet. This animal model was phenotyped using histopathology, clinical chemistry, microbiome and gene expression approaches. Data were compared to the phenotypes of human alcohol-related liver disease, including AH.

[*]Corresponding Author: Ivan Rusyn, MD PhD; 4458 TAMU, Texas A&M University, College Station, TX 77843, USA; Phone: +1-979-458-9866; irusyn@tamu.edu.

Disclosure. The authors have no conflicts to disclose.

Author Manuscript Author Manuscript Author Manuscript Author Manuscript

Results: Mice with cholestatic liver fibrosis and subsequent alcohol exposure (DDC+EtOH) exhibited exacerbated liver fibrosis with a pericellular pattern, increased neutrophil infiltration and ductular proliferation, all characteristics of human AH. DDC administration had no effect on urine alcohol concentration or liver steatosis. Importantly, DDC and alcohol treated mice showed a transcriptomic signature that resembled that of patients with AH. Finally, we show that mice in the DDC+EtOH group had an increased gut barrier dysfunction, mimicking an important pathophysiological mechanism of human AH.

Conclusions: We developed a novel mouse model of acute-on chronic cholestatic alcoholic liver injury that has considerable translational potential and can be used to test novel therapeutic modalities for AH.

Introduction

Excessive alcohol intake is a leading risk factor for global disease burden and is a major cause of preventable morbidity and mortality worldwide (Collaborators GBDA, 2018) due to adverse effects on multiple organs (Rusyn and Bataller, 2013), accidents, and violence (Rehm and Imtiaz, 2016). The liver is a major target organ for alcohol-induced disease (Szabo et al., 2019) and the spectrum of pathological states elicited by alcohol in liver comprises steatosis, alcoholic steatohepatitis (ASH), progressive fibrosis and cirrhosis, conditions that may progress to hepatocellular carcinoma (Seitz et al., 2018). Up to 90% of heavy drinkers develop hepatic steatosis, a condition that is usually asymptomatic and reversible with abstinence, with some of those progressing to ASH, fibrosis (20-40%) and cirrhosis (10-20%) (Lefkowitch, 2005). Alcohol-abusing patients can also develop alcoholic hepatitis (AH), a form of acute-on-chronic liver failure (Casanova and Bataller, 2014; Lucey et al., 2009). AH develops primarily in subjects with underlying cirrhosis (Altamirano et al., 2014) and is characterized by sudden worsening of clinical conditions – increase in serum bilirubin levels, jaundice and liver-related complications.

The mechanisms of alcohol-induced liver disease are complex and involve liver parenchymal and non-parenchymal cells, other cell types recruited to the liver in response to damage and inflammation, as well as other organs such as the gut and its microflora (Arteel, 2003; Seki and Schwabe, 2015; Szabo and Bala, 2010). Mechanisms of hepatocyte damage by alcohol are multifactorial and include formation of cytotoxic acetaldehyde and reactive oxygen species, injurious cytokines and chemokines, endoplasmic reticulum stress, mitochondrial dysfunction, and cell death via apoptosis and necrosis (Nagy et al., 2016). Cell death and ensuing inflammation result in the development of liver fibrosis, a process that involves hepatic stellate cell activation (Seki and Schwabe, 2015). Alcohol consumption is also tightly associated with gut barrier dysfunction and changes in the composition of the intestinal microbiota (Hartmann et al., 2019; Zhou et al., 2019). The intricate connections between injurious effects of alcohol, liver fibrosis/cirrhosis and impairments of intestinal permeability are triggers for AH (Cresci et al., 2017). In addition, alcohol abuse and bacterial infections may precipitate acute-on-chronic liver disease through the effect of chronic alcohol consumption on immunosuppression (Arroyo et al., 2016; Chiang et al., 2013).

Author Manuscript Author Manuscript Author Manuscript Author Manuscript

There are several animal models for ASH (Arteel, 2010; Bertola et al., 2013; Lazaro et al., 2015; Ueno et al., 2012); they vary in duration, mode of alcohol administration and the degree and types of liver injury produced. While most of these animal models, regardless whether alcohol is administered through liquid diet or intragastrically, produce steatohepatitis and mild fibrosis, it is widely acknowledged that they largely fail to fully recapitulate key characteristics of severe forms of alcoholic liver disease, such as AH (Mandrekar et al., 2016; Nagy et al., 2016; Prado et al., 2016). A common approach to exacerbate alcohol-induced liver disease in rodents has been to increase the alcohol dose by combining intragastric feeding of alcohol or a liquid diet with high-dose gavage simulating the alcohol binge (Bertola et al., 2013; Lazaro et al., 2015). These studies only showed few features of acute-on-chronic liver injury in the form of pericellular fibrosis, PMN infiltration, hypoalbuminemia, and bilirubinemia. An alternative approach is to combine alcohol and fibrosis in mouse models that also achieved some of the key features of AH such as exacerbated fibrosis (Chiang et al., 2013; Furuya et al., 2019) and acute renal injury (Furuya et al., 2016). Indeed, a recent AASLD-EASL Joint Conference on Alcohol-Related Liver Disease and Alcoholic Hepatitis (Szabo et al., 2019) noted that "*animal models that accurately model human disease where cholestasis, inflammation, and fibrosis are present together*" remain to be an unmet need in mechanistic research on alcohol-associated liver disease. Therefore, this study was conceived to fill an important gap that hampers the development of novel targeted therapies. Here, we combined a chronic cholestatic liver fibrosis model induced by 3,5-diethoxycarbonyl-1,4-dihydrocollidine (DDC) (Mariotti et al., 2018) with a mouse model of intragastric alcohol feeding (Kono et al., 2000). We phenotyped liver injury, used metagenomics to characterize changes in gut microbiome, metabolomics to investigate the effects of alcohol and fibrosis on bile acid metabolism, and transcriptomics to compare the molecular signatures of the liver injury in this mouse model to human alcohol-associated liver disease.

Materials and Methods

Animals.

Male mice (C57BL/6J, 20-25 g, 13-14 weeks of age) were obtained from the Jackson Laboratory (Bar Harbor, ME) and housed in a clean, temperature-controlled environment with a 12-h light-dark cycle and were given free access to regular laboratory chow diet and water for housing in regular cages. Male mice were selected for several reasons. First, in most published papers on alcoholic hepatitis in humans (Louvet et al., 2018), two-third of patients are male. Second, we aimed to compare the results from the mouse model detailed here to the previous study of a cytotoxic model of mouse alcoholic hepatitis (Furuya et al., 2019). All animals were given humane care in compliance with the National Institutes of Health guidelines. The degree of alcohol intoxication was assessed to evaluate the development of tolerance using a 0-3 behavioral scoring system. These studies were approved by the Institutional Animal Care and Use Committee at Texas A&M University.

Treatments.

Upon receipt from the vendor, mice were acclimated for 2 weeks on standard lab rodent chow with free access to food and water. At the beginning of the experiment (Figure 1A),

Author Manuscript Author Manuscript Author Manuscript Author Manuscript

mice were placed on 3,5-diethoxycarbonyl-1,4-dihydrocolidine (DDC)-containing (AD5002; grain-based rodent diet, 4.5% fat, 0.05% DDC, ½" pellets) or control (AD3012; grain-based rodent diet, 4.5% fat, ½" pellets) diets (Custom Animal Diets, Bangor, PA) with free access to food/water for 8 weeks. After 8 weeks of treatment, some of the animals were sacrificed while other animals were placed on control diet for 2 weeks. All of these animals underwent surgical intragastric intubation (Kono et al., 2000) at the beginning of week 10 of the study (Figure 1A). Following surgery, mice were housed in individual metabolic cages and allowed 1 week to recover with free access to control diet, water and non-nutritious cellulose pellets. At the start of week 11, groups of mice received through the gastric cannula (Kono et al., 2000) high-fat diets (HFD) prepared as detailed (Thompson and Reitz, 1978). Diets contained either maltose-dextrin (isocaloric control) or ethyl alcohol (EtOH, 190 proof, Koptec, VWR, Radnor, PA). The high-fat (corn oil-based) diet is necessary to facilitate alcohol-induced liver injury (Nanji et al., 1989). Alcohol was delivered (Figures 1B–C) continuously through the intragastric cannula initially at 14 g/kg/day and was gradually increased 1 g/kg every 2 days until day 14. The dose was then increased by 1 g/kg every 3 days up to 24 g/kg/day.

Eight experimental groups (n=4-8 animals per group) comprised this study (Figure 1A). Control ("Cont") group are animals that were fed control diet for 8 weeks and sacrificed, or animals that were also subject to intagastric tube implantation but were fed control diet for 4 weeks. "DDC" group are animals that were fed DDC (0.05%) diet for 8 weeks and sacrificed. "HFD" group are animals that that were fed control diet for 8 weeks and then were administered HFD intragastrically for 4 weeks. "EtOH" group are animals that were that fed control diet for 8 weeks and then were administered alcohol intragastrically for 4 weeks. "DDC+Cont" group are animals that were fed DDC diet for 8 weeks and then fed control diet for 4 weeks. "DDC+HFD" group are animals that were fed DDC diet for 8 weeks and then were administered HFD intragastrically for 4 weeks. "DDC+EtOH" group are animals that that fed DDC diet for 8 weeks and then were administered alcohol intragastrically for 4 weeks.

Sample collection.

Animals were deeply anesthetized with pentobarbital (50 mg/kg, intraperitoneal injection) and sacrificed via exsanguination through the vena cava, which was the site of blood collection. Serum collection via Z-gel tubes (Sarstedt, Nümbrecht, Germany) was performed at sacrifice. Other tissues were excised, rinsed in PBS, blotted dry, weighed, and snap-frozen in liquid nitrogen. The liver left lobe was separated from the rest of the liver prior to freezing. Sections of the left and median lobes and kidney were fixed in formalin for histological examination. Urine was collected using metabolic cages every morning (at 9 am) after starting alcohol administration and stored at −20ºC until assayed. Alcohol concentration was determined by measuring absorbance (366 nm) resulting from the reduction of NAD+ to NADH by alcohol dehydrogenase.

Histopathological evaluation.

Tissues were embedded in paraffin, sectioned at 5 μm, and stained with hematoxylin and eosin (H&E) or Sirius Red according to standard protocols. Liver pathology was evaluated

Author Manuscript Author Manuscript Author Manuscript Author Manuscript

in a blind manner by a certified veterinary pathologist and scored using two scales. For alcohol-specific scale, scoring procedure as detailed in (Nanji et al., 1989) was used. MDB scoring was done for zone 1 or zones 1 plus 3 because MDBs are found preferentially in zone 1 in cholestasis. Hepatocyte ballooning was scored as 0-3 (0, none; 1, rare; 2, frequent; 3, abundant) and zonal location noted. Bile plugs and non-bile pigment deposition, and intraductal lithiasis were noted for location and semi quantified (0-3 and 0-4, respectively). Periductal fibrosis was scored as 0/1 (0, absent; 1, present). Steatosis was scored as 1-3 (1, below 1%; 2, 1%-5%; 3, over 5%). Finally, paraffin-embedded sections were stained for Sirius red and Masson trichrome stains. Quantitative analysis was performed using ImageJ (https://imagej.nih.gov/ij/) in five random fields at 100× magnification.

Immunohistochemistry.

Paraffin-embedded liver sections (5 μm thick) were stained with primary antibodies as follows: rabbit anti-myeloperoxidase (MPO; Abcam, Cambridge, MA; 1:50), rabbit anti-4-hydroxynonenal (4-HNE; Alpha Diagnostics, San Antonio, TX; 1:1000), mouse anti-cytokeratin 7 (CK7; Dako, Carpinteria, CA; 1:100), mouse anti-cytokeratin 19; Dako; 1:100), and rabbit anti-lamin; Dako; 1:400). Goat IgG HRP-conjugated antibody (Millipore, Billerica, MA; AP132P, 1:2000) was used as a secondary antibody. Dako Liquid DAB+ Substrate chromogen System (Dako) consisting of streptavidin-horseradish peroxidase and 3,3′-diaminobenzidine substrate was employed for visualization. Slides were counterstained with filtered Mayer's hematoxylin for 60 seconds. Negative controls were incubated with irrelevant serum or isotype-matched immunoglobulin instead of the specific antibody. Quantitative analysis was performed using ImageJ (https://imagej.nih.gov/ij/) in five random fields at 200× magnification.

Biochemical measurements.

Serum aminotransferase (ALT) levels and triglyceride in the liver tissue were determined spectrophotometrically with the Thermo Scientific Infinity ALT Liquid stable reagent (Thermo Electron, Melbourne, Australia) and Wako L-Type TG M (Wako diagnostic, Richmond, VA). Albumin concentration levels in the fecal were determined spectrophotometrically with the Mouse Albumin ELISA Quantitation Set (Bethyl Laboratories, Montgomery, TX).

Western blotting.

Total protein was isolated from 15-20 mg of pulverized left liver lobe and kidney using the T-PER Tissue Protein Extraction Kit (Thermo Fisher Scientific, Waltham, MA) and Halt Protease Inhibitor Single-Use Cocktail (100×; Thermo Fisher Scientific) according to the manufacturer's protocol. Protein content was measured using the Pierce BCA Protein Assay Kit (Thermo Fisher Scientific). Protein samples (30 μg/lane) were resolved on pre-cast 10% acrylamide/bisacrylamide gels (BioRad, Hercules, CA), electrophoresed, transferred to TurboBlot PVDF membranes (BioRad), blocked for 2 hr at RT (Odyssey Blocking Buffer, Li-Cor, Lincoln, NE), and incubated with the polyclonal rabbit cytochrome P450 2E1 (Cyp2e1, ab28146, Abcam), or polyclonal rabbit anti-*E. coli* (E. coli, Dako) overnight at 4ºC. Membranes were washed and incubated with goat anti-rabbit HRP-conjugated secondary antibody for 1 hr at RT and chemiluminescence was used as a detection method

Author Manuscript Author Manuscript Author Manuscript Author Manuscript

of bands using a C-digit blot scanner (LiCor; Lincoln, NE) according to manufacturer's protocol. Amido black staining of membranes was employed as additional confirmation of equal protein loading. Intensity of the bands was quantified with Image Studio Ver4.0 (LiCor).

Detection of bacterial DNA in liver.

DNA was isolated from liver tissue with DNeasy Blood&Tissue kits (Qiagen, Valencia, CA). PCR was performed using Taqman (Thermo Fisher Scientific) gene expression assay probe for *Rps18* (Mm02601778_g1), or custom-made probes for *E.coli* as shown in Supplemental Table 1 (Malinen et al., 2005). Expression of *Rps18* was used as a reference. Reactions were performed in a 96-well assay format using LightCycler 480 (Roche Applied Science, Indianapolis, IN).

Quantitative reverse transcription-PCR.

Total RNA was extracted from liver or terminal ileum using the RNeasy Mini kit (Qiagen). RNA concentrations were measured with NanoDrop ND-1000 spectrophotometer (NanoDrop Technologies, Wilmington, DE) and quality was verified using the Bio-Analyzer (Agilent Technologies, Santa Clara, CA). Polymerase chain reaction (PCR) was performed using 2 μl of RNA (50 ng/μL) in a 20 μL total reaction volume using Taqman probes (Thermo Fisher Scientific, see Supplemental Table 2). Reactions were performed in a 96-well assay format using LightCycler 480 (Roche).

Gut microbiota analysis.

16S rRNA sequencing was done from DNA isolated from whole cecal samples (n=4-7 animals per group). DNA extraction was performed as described previously (Bluemel et al., 2018). Samples were digested with proteinase K (Thermo Fisher Scientific), RNAse A (Qiagen) and 10% sodium dodecyl sulfate (Sigma-Aldrich, St. Louis, MO) at 55°C for 1 hr. Suspensions were homogenized in phenol (Thermo Fisher Scientific) and extracted using phenol/chloroform/isoamyl alcohol (Thermo Fisher Scientific) three times followed by one extraction with chloroform and sodium acetate buffer solution (Sigma-Aldrich). DNA was precipitated and washed using ethanol and resuspended in sterile water (Thermo Fisher Scientific). The DNA was amplified using primers that target the V1-V3 region of the 16S rRNA gene (Kozich et al., 2013) as detailed in (Wang et al., 2016). Amplicons were purified and sequenced using Illumina MiSeq sequencing using the dual index V3 chemistry 2 × 300 bp format (Illumina, San Diego, CA) following the manufacturer's protocol. Processing and analysis of sequence reads was conducted as previously described (Wang et al., 2016). Sequence reads are available under NCBI BioSamples SAMN05272668-SAMN05272702 under BioProject PRJNA325943.

Liver RNA sequencing and analysis.

Libraries for RNA-seq were prepared from total liver RNA using the Illumina TruSeq mRNA Sample Prep Kit (Illumina). Pair-end (100 bp) sequencing was carried out using the Illumina HiSeq 2500 platform. RNA-seq reads were aligned to appropriate reference genomes (NCBI mm10) using the "SNP-tolerant" GSNAP software. This alignment pipeline

Author Manuscript Author Manuscript Author Manuscript Author Manuscript

allows for the elimination of mapping biases that arise from discrepancies in genetic variation between individual samples and a standard reference genome, at both homozygous and heterozygous sites. Sequencing quality and mapping statistics were compared across all samples and duplicate entries and transcripts with less than 0 counts were removed. Differential gene expression tests were then performed using DESeq2 (Love et al., 2014) on the complete list of 18,965 expressed transcripts. To be deemed differentially-expressed transcripts, log2 fold-changes (compared to control) and false discovery rate (FDR)-adjusted p-values cut off were 0.585 and 0.1, respectively. RNA sequencing data are available at Gene Expression Omnibus (GSE119953).

Pathway annotation of the differentially expressed genes.

Gene Set Enrichment Analysis (Subramanian et al., 2007) was utilized to execute KEGG pathway (http://www.genome.jp/kegg/) analysis, annotation and analysis of related diseases on the DEGs. FDR q-value <0.05 and FWER p-value <0.05 were was considered as the significantly enriched threshold. The resulting gene expression values were used for biological pathway analysis using the *piano* package (Varemo et al., 2013) in conjunction with the “Mouse Reactome” gene set (www.baderlab.org). To identify in an unbiased way the transcription factors predicted to be directly involved on transcriptomic changes we used functional prediction of differentially expressed genes (DEG) by the use of Ingenuity Pathway Analysis (IPA, Qiagen, version 01-13), selecting among predicted upstream regulators, those involved in transcriptional regulation (categories: “transcriptional regulator”, “ligand-dependent nuclear receptor”). The top 1,000 differentially expressed genes for each comparison were used for IPA. A hypergeometric statistic was used to calculate the probability of a pre-defined set of transcription factor-target genes was enriched in the gene set of DEG, when compared to normal proportion accounting for the transcription factor-target gene set in the mouse transcriptome. The adjustment of this p-value was performed using the Benjamini & Hochberg method (Benjamini and Hochberg, 1995). The statistic approach used to calculate the predicted activation state (IPA) was z-score and is used to infer likely activation states of upstream regulators based on comparison with a model that assigns random regulation directions. Transcription factors selected for figure 6 had an adjusted p-value of the overlap of less than 10^{-4} and a Z-Score >2 (for those predicted to be upregulated) or <−2 (for those predicted to be downregulated). To compare the present model with a previously published model of CCl_4 and ethanol treatment (Furuya et al., 2019), the raw counts were downloaded from Gene Expression Omnibus (GSE119953). Raw counts of both sets of experiments were normalized using voom function in limma package (v 3.40.6) (Ritchie et al., 2015). Heatmaps of Hnf4a target genes were assembled using pheatmap R package (v1.0.12).

Statistical analyses.

Comparisons among groups for all phenotypes except for gene expression was conducted using Prizm (v.7, GraphPad Software, San Diego, CA). Statistical significance was established using t-test or one-way ANOVA methods ($p<0.05$) as stated in the figure legends.

Author Manuscript Author Manuscript Author Manuscript Author Manuscript

Results

Develovment of a model of acute-on chronic cholestatic alcoholic liver injury.

This study aimed to evaluate pathophysiological and molecular effects of alcohol-induced liver injury with existing chronic cholestatic fibrosis, to mimic the human disease (Mandrekar et al., 2016; Szabo et al., 2019). Because human AH is characterized by exacerbated fibrosis and cholestasis on a chronically damaged liver, and alcohol *per se* in unable to cause advanced liver disease in mice, we first induced chronic liver fibrosis using a cholestatic DDC model (Mariotti et al., 2018). Animals were placed on DDC (0.05%)-containing diet for 8 weeks (Figure 1A). After a washout period, mice underwent intragastric intubation (Kono et al., 2000) and administration of no liquid diet, or liquid diet containing high fat with or without alcohol (up to 24 g/kg/day). Overall, this study comprised 8 experimental groups in order to enable differential analysis between normal liver, cholestatic liver injury, high fat diet, alcohol, and combinations of several factors.

In the intragastric alcohol groups, alcohol content in the liquid diet was increased gradually from 16 g/kg/day to 24 g/kg/day over a period of 16 days (Figures 1B–C, dotted line). Due to poor tolerance of rapid increases in alcohol content (animals were found to be lethargic for extended periods of time), the dose was decreased to 22 g/kg/day on day 17 and then gradually increased to 24 g/kg/day in 3-day increments allowing for a longer period to develop tolerance until termination of the study at day 28 or alcohol treatment (14 weeks of the overall experiment). Importantly, no differences were observed between animals in EtOH and DDC+EtOH in alcohol cycling, peak and average urine alcohol levels (Figure 1B), or degree of inebriation (Figure 1C). This indicates that administration of DDC did not affect alcohol metabolism and circulating levels. Similarly, alcohol-induced fat content in liver, as measured by liver triglyceride levels (Figure 1D), and liver CYP2E1 protein amounts (Figure 1E) were markedly elevated in both EtOH-treated groups as expected and were indistinguishable from each other.

Liver injury and histological analysis of the model.

Liver injury was evaluated using histopathology, specialty stains for collagen, and immunohistochemical staining (Figure 2 and Supplemental Figure 1). As expected, administration of 0.05% DDC for 8 weeks caused cholestasis-associated peri-portal fibrosis with some pericellular collagen deposition and lipid peroxidation, as evidenced by diffuse staining with 4-HNE. Intragastric feeding with alcohol (EtOH group) produced marked steatohepatitis (as evidenced by the accumulation of fat droplets and macrophage staining), but only moderate lipid peroxidation and little increase in collagen staining. In the animals treated with DDC for 8 weeks and maintained on a control diet for additional 6 weeks (DDC +Cont group), periportal collagen deposition remained, but peri-cellular collagen deposits were largely absent; lipid peroxidation levels remained high. Finally, in the EtOH+DDC group, the alcohol effects on fat accumulation, oxidative stress and macrophage infiltration were as high or greater than those in the EtOH group; however, pronounced liver fibrosis, both peri-portal and peri-cellular, was prominent. This finding closely mimics typical histological features in humans with AH (Altamirano et al., 2014). No effects of either DDC or EtOH were found in the kidneys of mice in this study (Supplemental Figure 2).

Author Manuscript Author Manuscript Author Manuscript Author Manuscript

Quantitative analysis of the biomarkers of liver injury and quantitative analysis of the histopathological effects are presented in Figure 3. As expected, serum ALT levels (Figure 3A) were elevated in animals receiving DDC diet, but decreased to control levels in DDC +Cont group. Both EtOH-treated groups showed increases in serum ALT indicative of continued liver injury. Liver enlargement (Figure 3B) followed the same trends. Liver histopathological evaluation was conducted using two different scoring methods. The so-called Nanji scoring method (Nanji et al., 1989) is tailored to rodent models of alcohol-induced liver injury and weighs fat accumulation more than inflammation and necrosis. Not surprisingly, EtOH-treated groups scored much higher than even the DDC group (Figure 3C), and the EtOH+DDC group average was higher than that of EtOH alone group, albeit no significant difference present. A more traditional veterinary pathology evaluation of liver injury (Figure 3D) demonstrated that upon removal of DDC, liver injury subsides (DDC vs DDC+Cont groups); however, alcohol administration maintains high degree of liver injury, significantly greater than that in EtOH alone group.

Evaluation of liver fibrosis using two stains showed that Sirius red-positive areas remain elevated in all animals treated with DDC (Figure 3E). Masson trichrome stained areas declined considerably after cessation of DDC treatment, except for the EtOH+DDC group (Figure 3F). We note that while image analysis allows for evaluation of stained areas, the patterns of staining, such as pronounced peri-cellular fibrosis in EtOH+DDC group, are difficult to ascertain quantitatively; therefore, the qualitative analysis presented in Figure 2 may be a better indicator of the fibrosis changes in these models. Finally, lipid peroxidation (Figure 3G) and neutrophil infiltration (Figure 3H) followed similar trends whereby EtOH, DDC or combination of the two exhibited significant elevation in these markers of oxidative stress and inflammation; greatest injury was detected immediately after cessation of DDC treatment and in EtOH+DDC group.

Progenitor cell expansion.

To characterize the cellular pathways that are affected in mice receiving alcohol in a background of fibrotic liver, we evaluated the presence of progenitor ductular cell reaction, a typical feature of human AH (Aguilar-Bravo et al., 2019; Dubuquoy et al., 2015; Odena et al., 2016). These studies identified several keratins (KRT23, KRT19, and KRT7), proteins that mediate hepatic progenitor cell (HPC) differentiation, as markedly upregulated in AH. Not only they were among the most upregulated genes in human AH compared to NASH and normal livers, but also they were found to be markedly induced in a mouse cholestatic liver fibrosis model and mildly upregulated in the intragastric alcohol feeding model (Odena et al., 2016). Expansion of progenitor cells that poorly differentiate into mature hepatocytes, the so-called ductular reaction, is a feature of poor prognosis of human AH (Altamirano et al., 2012; Dubuquoy et al., 2015). Therefore, we first assessed expression of cytokeratins 7 (*Krt7*) and 23 (*Krt23*), markers of the ductular reaction that is typically composed of HPC engaged in cholangiocyte differentiation. Figures 4A–B show that livers from mice on DDC diet exhibited marked upregulation of both markers. Expression was largely unaffected by either alcohol or high fat diet, and reverted back to control levels after DDC feeding ceased. However, in mice with both non-alcoholic and alcoholic liver injury on a fibrotic liver background, both markers remained upregulated, especially in the EtOH+DDC group.

Author Manuscript Author Manuscript Author Manuscript Author Manuscript

To map cells overexpressing these HPC markers in the liver, we conducted immunohistochemical evaluation (Figure 4C). We stained for KRT7 and KRT19, which can also identify HPCs that are fated biliary cells (Dubuquoy et al., 2015). In control animals and animals treated with alcohol alone, we detected cytokeratins 7 and 19 only in the bile ducts in portal areas; however, pronounced ductular reaction was noticed in periportal areas in DDC-treated mice and, albeit to a lesser degree, in animals of DDC+HFD and DDC +EtOH groups. Overall, these results indicated that mouse liver fibrosis induced by DDC is characterized by a massive yet inefficient accumulation of HPC of predominantly biliary phenotype and that both non-alcoholic and alcoholic injury slows down resolution of the ductular reaction. To determine potential mechanisms that may favor cholangiocyte differentiation of HPC in this model, we evaluated laminin, extracellular matrix protein that promotes cholangiocyte differentiation. Patterns of protein expression of laminin largely followed those of KRT7 and KRT19, surrounding the ductular reaction and also present in the sunisoids, an observation that is similar to findings in human AH (Aguilar-Bravo et al., 2019; Dubuquoy et al., 2015).

Comparative transcriptome analysis with human AH.

We recently reported a comprehensive analysis of liver RNA sequencing data from a large number of patients (N=92) with different disease stages including normal liver, early ASH, AH with liver failure, and a unique set of explants from patients with AH that underwent early liver transplantation (Argemi et al., 2019). A comparative analysis of liver transcriptomic changes in a mouse model of cytotoxic fibrosis-associated alcohol-induced liver injury (carbon tetrachloride-induced fibrosis combined with intragastric alcohol feeding) showed some similarities with pathways perturbed in patients with severe AH (Furuya et al., 2019). Here, we sought to characterize the molecular pathways and similarities of the model developed in this study to human AH, or to the mouse model of the cytotoxic fibrosis-associated alcohol-induced liver injury.

We compared significantly affected transcripts in severe human AH and in the DDC+EtOH group in the mouse and identified 685 transcripts that were shared across species (Figure 5A). Similar comparison of the mouse significant transcripts was done to the data from non-severe human AH; this analysis yielded 447 transcripts. About half of the transcripts were common between the two lists and the union of these two analyses comprised 735 transcripts that were further interrogated for species comparisons. Principal component analysis of the individual samples, from either human or mouse livers, based on the gene expression data of the 735 transcripts (Figure 5B) showed that the transcriptomic signature of the mouse model overlapped most closely with non-severe human AH. However, it is also evident that there is a gradient of severity of AH among human samples based on transcriptional signatures.

We also used transcriptomic data on the union of the identified genes to conduct sample clustering analysis (Figure 5C). All samples from the mouse model detailed herein were included in this analysis to determine what treatment groups may be most concordant with human AH. Similar to the principal component analysis on Figure 5B, we show that all human AH samples exhibited highly similar patterns in up- and down-regulated transcripts and that mouse DDC+EtOH group is most closely reflective of the human transcriptional

Author Manuscript Author Manuscript Author Manuscript Author Manuscript

responses. As expected, the transcriptomic profile mice without pre-existing liver injury exposed to EtOH group largely differ from human AH.

Transcripts in 6 clusters that separated human and mouse liver gene expression signatures were further analyzed for the enrichment of pathways (Table 1). Importantly, the overall transcriptome changes in mice with pre-existing advanced liver fibrosis (*i.e.*, DDC model of cholestatic liver injury) plus EtOH showed marked similarities with human AH. In particular, up-regulated pathways that were shared between mouse DDC+EtOH group and human AH samples were largely related to fibrogenesis, indicating that despite withdrawal of DDC, alcohol treatment in the mouse retards resolution of fibrosis and maintains the ductular reaction. In addition, the negative regulation of chemotaxis shared among species is a known mechanism in rodent alcohol-induced injury (Bautista, 2002). Common down-regulated pathways are also well established factors that, when dysregulated, exacerbate liver injury by alcohol. These include PPAR signaling (Tsukamoto, 2015), cholesterol biosynthesis (Brandl et al., 2018; Hirsova et al., 2016), and the complement cascade (Bird et al., 1995). Interestingly, human AH was associated with a much more pronounced transcriptional response to LPS, also a known modulator of severe human AH (Argemi et al., 2019; Hartmann et al., 2015). A discordant response between mouse and human severe liver injury was upregulation of xenobiotic metabolism in the mouse, yet drug metabolism pathways are commonly downregulated in human AH. These findings were similar to those observed in the carbon tetrachloride-associated fibrosis and alcohol model (Furuya et al., 2019).

Transcription factors and nuclear receptor are main expression regulators and its activity can be predicted by the inference of the activation or inhibition of their target genes. Recently, a suppression of liver-enriched transcription factor transcriptional signature has been associated with the progression of AH (Argemi et al., 2019). Therefore, we aimed to compare (Figure 6) liver transcription factor signature of the DDC+EtOH model to that of the mouse model of the cytotoxic fibrosis-associated alcohol-induced liver injury (Furuya et al., 2019). When treated with EtOH alone, the characteristic downregulation of liver-enriched transcription factors previously described in human AH was not observed (Figure 6A). To the contrary, in mice treated with DDC alone, significant inhibition of the transcripts that are under control of HNF4A and other liver-specific transcription factors such as HNF1A and RXRA was observed (Figure 6B). These effects were indicative of the disruption in hepatic metabolism and promotion of cell proliferation, pathways known to be affected in liver fibrosis (Cicchini et al., 2015). In DDC+EtOH group, the signature of HNF4A remained downregulated, while the footprint of other liver enriched transcription factors did not reach statistical significance (Figure 6B). It is noteworthy that there was considerable similarity in the transcription factor signature between EtOH and DDC+EtOH groups (Figures 6A and C), such as inhibition of STAT5B, a hepatoprotective JAK2-dependent transcription factor, and activation of NRF2 (NFE2L2), which is a key regulator of oxidative stress (Sun et al., 2018). The inhibition of HNF4A and activation of JUN and TP53 are also affected in human AH in the same direction (Argemi et al., 2019). The fact that HNF4A signature remained partially downregulated in mice after cessation of DDC treatment suggests that alcohol inhibits resolution of the fibrosis-associated molecular changes. In contrast, CCl_4-only and CCl_4+EtOH treated mice could only partially reproduce

Author Manuscript Author Manuscript Author Manuscript Author Manuscript

this liver-enriched TF downregulation. Interestingly, these mice presented inhibition of HNF4A coactivator PPARGC1A and some of the HNF4A targets (Figures 6D and 6E). Although the expression of a transcription does not always correlate with its function, we found lower expression of Hnf4a mRNA only in DDC-treated mice (Argemi et al., 2019). However, a signature of downregulated transcription factor HNF4A was evident in the down-regulation of its targets (Figure 6F). Specifically, in the DDC+EtOH group these included clotting factors (F7), amino acid metabolism (Hal, Tars, Grhpr), genes of the cytochrome P450 system responsible for drug metabolism (Cyp2a1, Hsd11b1), bile acid and cholesterol metabolism (Cyp8a1, Cyp7b1), bile acid transport (Slc10a1 or Ntcp), fatty acid metabolism (Acsl1, Fabp1). Some of the HNF4A target genes were also down regulated in both DDC+EtOH and CCL_4+EtOH animals (Figure 6G). Collectively, these data indicate that the addition of cholestatic syndrome to ethanol damage in DDC+EtOH mice partially mimics the transcriptional reprogramming occurring in the liver of patients with AH.

Microbiome analysis.

We characterized the gut microbiome in this mouse model because microbiota changes have been associated with liver injury in models of chronic alcohol administration in mice (Bluemel et al., 2019; Zhou et al., 2019). Figure 7A depicts the colonization pattern of the 20 most prevalent bacteria isolated from the feces of the individual animals in this study. While inter-individual variability in bacterial colonization pattern was evident in each treatment group, there were distinct effects of the high-fat diet, independent of treatments with EtOH or DDC, on the gut microbiota. Specifically, the relative abundance of *Lachnospiraceae* species was reduced while *Ruminococcaceae*, *Porphyromonadaceae*, *Akkermansia*, and *Allobaculum* species were increased. Species richness and alpha-diversity results for the fecal microbiome are shown in Figure 7B. The overall microbial species richness was significantly lower in DDC-treated animals that received high fat diet, with or without alcohol, compared to other groups; Chao1 index showed the same pattern. Low Shannon and high Simpson indices show that the diversity of the species was reduced in samples from groups treated with the high fat diet, regardless of the presence of alcohol or DDC.

Next, we determined the state of the gut barrier by examining fecal albumin, Ocln mRNA and serum and liver LPS binding protein abundance (Figure 7C). We find that the animals in the DDC+EtOH group had the most “leaky” gut barrier as evidenced from fecal albumin and serum LPS binding protein levels that were significantly higher in this group as compared to others, even though occludin expression and liver LPS binding protein levels were similar to other groups. In addition, liver load of bacterial DNA and *E. coli* protein abundance were significantly higher in the DDC+EtOH group (Figure 7D). However, based on the gut microbiome analysis (Figure 7A) of the abundance of Gram+ vs Gram− species, we found that DDC treatment is associated with increased Gram−, but there does not seem to be a difference between DDC+HFD and DDC+EtOH groups (Figure 7D).

Author Manuscript Author Manuscript Author Manuscript Author Manuscript

Discussion

The search for a suitable animal model of human acute AH is an urgent need since it is currently considered a barrier for the development of novel therapies (Szabo et al., 2019). Most commonly used animal models of alcohol-induced liver disease reflect the presence of liver damage and steatohepatitis, but they lack severe pericellular fibrosis, cholestatic features and liver synthetic dysfunction (Gao and Bataller, 2011; Seitz et al., 2018). Because the degree of fibrosis and cholestasis in humans are predictive factors of early mortality, it is imperative to develop animal models that include, at least in part, these important features. With the present work, we aimed to provide a more suitable animal model to replicate the pathophysiology of human disease so that the molecular drivers can be better understood; a model that can be used to test novel therapeutic strategies for human AH.

Besides analytical and histological similarities between our new model and patients with AH, we performed extensive cellular and molecular comparative analysis. First, we assessed whether our model of acute-on-chronic ALD develops ductular reaction, a hallmark finding in patients with AH that has also predictive value (Sancho-Bru et al., 2012). The histological and gene expression analysis clearly show that alcohol exposure to fibrotic livers markedly induced the accumulation of ductular cells. Because these cells display an inflammatory phenotype and are not efficient in regenerating the liver, our model represents a new tool to test strategies to limit this futile cellular reaction of the failing liver (Aguilar-Bravo et al., 2019). Genes involved in the fibrogenic response in human AH were also markedly up-regulated in our new mouse model. This finding, along with the “chicken-wire” pattern of liver fibrosis found in mice exposed to DCC+EtOH, makes our experimental model a unique tool to study new strategies to reduce liver fibrosis in AH. In fact, we previously demonstrated that the degree of liver fibrosis closely correlates with the clinical outcome in these patients, reinforcing the need to develop effective antifibrotic therapies in this setting (Altamirano et al., 2014).

In order to globally compare the molecular changes in the different human and mice phenotypes, we performed an integrative transcriptome analysis. The functional enrichment analysis of the transcriptomic changes showed the commonalities between human AH and mouse DDC+EtOH transcriptomes, including the downregulation of key hepatocyte specific pathways like cholesterol and clotting factor biosynthesis and the upregulation of fibrosis-related genes and cell proliferation. Interestingly, most of the patients affected by AH have advanced fibrosis and, mostly due to ductular proliferation, exhibit characteristic hepatomegaly.

Another striking similarity between human AH and mice subjected to DDC+EtOH treatment are changes in the intestinal microbiome. Based on unbiased qualitative analysis of feces, the microbiota is not much different between DDC+HFD and DDC+EtOH mice, although for some species the groups of animals treated with HFD exhibited particular changes, regardless the presence of DDC or EtOH. Despite the similarities between DDC+HFD and DDC+EtOH, the bacterial translocation and the gut permeability, as shown by a higher presence of circulating pan-bacterial DNA, *E. coli* protein abundance and serum LPS binding protein, were highest in the DDC+EtOH group. Whether these differences could be

Author Manuscript Author Manuscript Author Manuscript Author Manuscript

involved in the increased ductular fibrosis and the pattern of perisinusoidal “chicken-wire” fibrosis deserves future investigation. Regarding the specific mechanism of gut permeability in this model, further research will also need to address the potential role of local intestinal inflammation, or rather the systemic inflammatory responses. An interesting finding is that gram negative bacteria globally seem to have similar increased proportion in both DDC +HFD and DCC+EtOH models, while, as stated before, the amount of serum LBP is higher in the latter, a difference that could be attributed to the different qualitative translocated microbiome composition.

There are several limitations of the animal model detailed herein is the lack of profound hepatocellular synthetic dysfunction and liver failure. Studies in animals cannot be conducted with death (i.e., liver failure) as an endpoint; therefore, the dose of alcohol was closely monitored and had to be scaled back temporarily after 2.5 weeks (Figure 1B) to mitigate pain and distress. In addition, our analysis of the transcription factor changes is also informative as combined administration of DDC and alcohol is able to induce cholestasis and extensive fibrosis, but the basic liver function is still preserved. We recently demonstrated that defective HFN4A-dependent gene expression plays a key role in hepatocellular failure in patients with AH (Argemi et al., 2019). We explored the predicted activation of transcriptional regulators in all mouse phenotypes, and compared them with the recently published human data. DDC-induced fibrosis was associated with decreased predicted activity of HNF1A, RXRA and, more importantly, HNF4A. Addition of alcohol after a brief washout period induced deregulated transcription factor activation. Remarkably, while some changes resembled the findings in human AH (i.e., RXRA inhibition), the decreased activation of HNF4A induced by DDC alone was not fully observed in DDC +EtOH group. This result could partially explain the lack of profound hepatocellular dysfunction in this mouse model. It also suggests that the cessation, even for brief period, of a fibrogenic insult such as DDC results in rapid recovery of the normal hepatocellular homeostasis. Still, these results show that the DDC+EtOH model resembles human disease with higher fidelity than CCL4+EtOH model previously reported (Argemi et al., 2019; Furuya et al., 2019). Based on these results, we hypothesize that interfering with HNF4A in DDC-EtOH model could favor the development of all the features of AH in mice subjected to alcoholic acute-on-chronic liver injury, thus resulting in a more human-relevant animal model.

In conclusion, we report on the development of a new mouse model of acute-on-chronic liver injury in which alcohol was administered subsequently to established cholestatic liver fibrosis. We provide evidence that despite limitations this model exhibits key clinical, histological and molecular features similar to patients with AH. This preclinical model represents a new tool to test targeted therapies to attenuate advanced alcohol-induced liver injury; however, this model requires intragastric alcohol feeding which is a technically challenging procedure and the utility of this model may be limited. Further studies should evaluate additional animal models (*i.e.*, transgenic mice, humanized mouse livers, etc.) to achieve a more profound liver dysfunction.

Author Manuscript Author Manuscript Author Manuscript Author Manuscript

Supplementary Material

Refer to Web version on PubMed Central for supplementary material.

Acknowledgements.

The authors thank Dr. Joseph A. Cichocki and Dr. Kranti Konganti for technical assistance in the conduct of these studies. This work was funded, in part, by grants from NIH (U01 AA021908, R01 AA016258).

References

Aguilar-Bravo B, Rodrigo-Torres D, Arino S, Coll M, Pose E, Blaya D, Graupera I, Perea L, Vallverdu J, Rubio-Tomas T, Dubuquoy L, Armengol C, Lo Nigro A, Starkel P, Mathurin P, Bataller R, Caballeria J, Jose Lozano J, Gines P, Sancho-Bru P (2019) Ductular Reaction Cells Display an Inflammatory Profile and Recruit Neutrophils in Alcoholic Hepatitis. Hepatology 69(5):2180–2195. [PubMed: 30565271]

Altamirano J, Fagundes C, Dominguez M, Garcia E, Michelena J, Cardenas A, Guevara M, Pereira G, Torres-Vigil K, Arroyo V, Caballeria J, Gines P, Bataller R (2012) Acute kidney injury is an early predictor of mortality for patients with alcoholic hepatitis. Clin Gastroenterol Hepatol 10(1):65–71. [PubMed: 21946124]

Altamirano J, Miquel R, Katoonizadeh A, Abraldes JG, Duarte-Rojo A, Louvet A, Augustin S, Mookerjee RP, Michelena J, Smyrk TC, Buob D, Leteurtre E, Rincon D, Ruiz P, Garcia-Pagan JC, Guerrero-Marquez C, Jones PD, Barritt ASt, Arroyo V, Bruguera M, Banares R, Gines P, Caballeria J, Roskams T Nevens F, Jalan R, Mathurin P, Shah VH, Bataller R (2014) A histologic scoring system for prognosis of patients with alcoholic hepatitis. Gastroenterology 146(5):1231–1239. [PubMed: 24440674]

Argemi J, Latasa MU, Atkinson SR, Blokhin IO, Massey V, Gue JP, Cabezas J, Lozano JJ, Van Booven D, Bell A, Cao S, Vernetti LA, Arab JP, Ventura-Cots M, Edmunds LR, Fondevilla C, Starkel P, Dubuquoy L, Louvet A, Odena G, Gomez JL, Aragon T, Altamirano J, Caballeria J, Jurczak MJ, Taylor DL, Berasain C, Wahlestedt C, Monga SP, Morgan MY, Sancho-Bru P, Mathurin P, Furuya S, Lackner C, Rusyn I, Shah VH, Thursz MR, Mann J, Avila MA, Bataller R (2019) Defective HNF4alpha-dependent gene expression as a driver of hepatocellular failure in alcoholic hepatitis. Nat Commun 10(1):3126. [PubMed: 31311938]

Arroyo V, Moreau R, Kamath PS, Jalan R, Gines P, Nevens F, Fernandez J, To U, Garcia-Tsao G, Schnabl B (2016) Acute-on-chronic liver failure in cirrhosis. Nat Rev Dis Primers 2:16041. [PubMed: 27277335]

Arteel GE (2003) Oxidants and antioxidants in alcohol-induced liver disease. Gastroenterology 124(3): 778–790. [PubMed: 12612915]

Arteel GE (2010) Animal models of alcoholic liver disease. Dig Dis 28(6):729–36. [PubMed: 21525757]

Bautista AP (2002) Chronic alcohol intoxication primes Kupffer cells and endothelial cells for enhanced CC-chemokine production and concomitantly suppresses phagocytosis and chemotaxis. Front Biosci 7:a117–25. [PubMed: 12045006]

Benjamini Y, Hochberg Y (1995) Controlling the False Discovery Rate - a Practical and Powerful Approach to Multiple Testing. J Roy Stat Soc B Met 57(1):289–300.

Bertola A, Mathews S, Ki SH, Wang H, Gao B (2013) Mouse model of chronic and binge ethanol feeding (the NIAAA model). Nat Protoc 8(3):627–37. [PubMed: 23449255]

Bird GL, Lau JY, Davies ET, Williams RS (1995) Lack of plasma complement activation in severe acute alcoholic hepatitis. Alcohol Clin Exp Res 19(6):1537–40. [PubMed: 8749823]

Bluemel S, Wang L, Kuelbs C, Moncera K, Torralba M, Singh H, Fouts DE, Schnabl B (2019) Intestinal and hepatic microbiota changes associated with chronic ethanol administration in mice. Gut Microbes:1–11.

Author Manuscript Author Manuscript Author Manuscript Author Manuscript

Bluemel S, Wang L, Martino C, Lee S, Wang Y, Williams B, Horvath A, Stadlbauer V, Zengler K, Schnabl B (2018) The Role of Intestinal C-type Regenerating Islet Derived-3 Lectins for Nonalcoholic Steatohepatitis. Hepatol Commun 2(4):393–406. [PubMed: 29619418]

Brandl K, Hartmann P, Jih LJ, Pizzo DP, Argemi J, Ventura-Cots M, Coulter S, Liddle C, Ling L, Rossi SJ, DePaoli AM, Loomba R, Mehal WZ, Fouts DE, Lucey MR, Bosques-Padilla F, Mathurin P, Louvet A, Garcia-Tsao G, Verna EC, Abraldes JG, Brown RS Jr, ., Vargas V, Altamirano J, Caballeria J, Shawcross D, Starkel P, Ho SB, Bataller R, Schnabl B (2018) Dysregulation of serum bile acids and FGF19 in alcoholic hepatitis. J Hepatol 69(2):396–405. [PubMed: 29654817]

Casanova J, Bataller R (2014) Alcoholic hepatitis: Prognosis and treatment. Gastroenterol Hepatol 37(4):262–8. [PubMed: 24656653]

Chiang DJ, Roychowdhury S, Bush K, McMullen MR, Pisano S, Niese K, Olman MA, Pritchard MT, Nagy LE (2013) Adenosine 2A receptor antagonist prevented and reversed liver fibrosis in a mouse model of ethanol-exacerbated liver fibrosis. PLoS One 8(7):e69114. [PubMed: 23874883]

Cicchini C, Amicone L, Alonzi T, Marchetti A, Mancone C, Tripodi M (2015) Molecular mechanisms controlling the phenotype and the EMT/MET dynamics of hepatocyte. Liver Int 35(2):302–10. [PubMed: 24766136]

Collaborators GBDA (2018) Alcohol use and burden for 195 countries and territories, 1990-2016: a systematic analysis for the Global Burden of Disease Study 2016. Lancet 392(10152):1015–1035. [PubMed: 30146330]

Cresci GA, Glueck B, McMullen MR, Xin W, Allende D, Nagy LE (2017) Prophylactic tributyrin treatment mitigates chronic-binge ethanol-induced intestinal barrier and liver injury. J Gastroenterol Hepatol 32(9):1587–1597. [PubMed: 28087985]

Dubuquoy L, Louvet A, Lassailly G, Truant S, Boleslawski E, Artru F, Maggiotto F, Gantier E, Buob D, Leteurtre E, Cannesson A, Dharancy S, Moreno C, Pruvot FR, Bataller R, Mathurin P (2015) Progenitor cell expansion and impaired hepatocyte regeneration in explanted livers from alcoholic hepatitis. Gut 64(12):1949–60. [PubMed: 25731872]

Furuya S, Chappell GA, Iwata Y, Uehara T, Kato Y, Kono H, Bataller R, Rusyn I (2016) A mouse model of alcoholic liver fibrosis-associated acute kidney injury identifies key molecular pathways. Toxicol Appl Pharmacol 310:129–139. [PubMed: 27641628]

Furuya S, Cichocki JA, Konganti K, Dreval K, Uehara T, Katou Y, Fukushima H, Kono H, Pogribny IP, Argemi J, Bataller R, Rusyn I (2019) Histopathological and molecular signatures of a mouse model of acute-on-chronic alcoholic liver injury demonstrate concordance with human alcoholic hepatitis. Toxicol Sci 170:427–437. [PubMed: 30517762]

Gao B, Bataller R (2011) Alcoholic liver disease: pathogenesis and new therapeutic targets. Gastroenterology 141(5):1572–85. [PubMed: 21920463]

Hartmann P, Chu H, Duan Y, Schnabl B (2019) Gut microbiota in liver disease: too much is harmful, nothing at all is not helpful either. Am J Physiol Gastrointest Liver Physiol 316(5):G563–G573. [PubMed: 30767680]

Hartmann P, Seebauer CT, Schnabl B (2015) Alcoholic liver disease: the gut microbiome and liver cross talk. Alcohol Clin Exp Res 39(5):763–75. [PubMed: 25872593]

Hirsova P, Ibrahim SH, Krishnan A, Verma VK, Bronk SF, Werneburg NW, Charlton MR, Shah VH, Malhi H, Gores GJ (2016) Lipid-Induced Signaling Causes Release of Inflammatory Extracellular Vesicles From Hepatocytes. Gastroenterology 150(4):956–67. [PubMed: 26764184]

Kono H, Bradford BU, Rusyn I, Fujii H, Matsumoto Y, Yin M, Thurman RG (2000) Development of an intragastric enteral model in the mouse: studies of alcohol-induced liver disease using knockout technology. J Hepatobiliary Pancreat Surg 7(4):395–400. [PubMed: 11180860]

Kozich JJ, Westcott SL, Baxter NT, Highlander SK, Schloss PD (2013) Development of a dual-index sequencing strategy and curation pipeline for analyzing amplicon sequence data on the MiSeq Illumina sequencing platform. Appl Environ Microbiol 79(17):5112–20. [PubMed: 23793624]

Lazaro R, Wu R, Lee S, Zhu NL, Chen CL, French SW, Xu J, Machida K, Tsukamoto H (2015) Osteopontin deficiency does not prevent but promotes alcoholic neutrophilic hepatitis in mice. Hepatology 61(1):129–40. [PubMed: 25132354]

Lefkowitch JH (2005) Morphology of alcoholic liver disease. Clin Liver Dis 9(1):37–53. [PubMed: 15763228]

Author Manuscript Author Manuscript Author Manuscript Author Manuscript

Louvet A, Thursz MR, Kim DJ, Labreuche J, Atkinson SR, Sidhu SS, O'Grady JG, Akriviadis E, Sinakos E, Carithers RL Jr, Ramond MJ, Maddrey WC, Morgan TR, Duhamel A, Mathurin P (2018) Corticosteroids Reduce Risk of Death Within 28 Days for Patients With Severe Alcoholic Hepatitis, Compared With Pentoxifylline or Placebo-a Meta-analysis of Individual Data From Controlled Trials. Gastroenterology 155(2):458–468 e8. [PubMed: 29738698]

Love MI, Huber W, Anders S (2014) Moderated estimation of fold change and dispersion for RNA-seq data with DESeq2. Genome Biol 15(12):550. [PubMed: 25516281]

Lucey MR, Mathurin P, Morgan TR (2009) Alcoholic hepatitis. N Engl J Med 360(26):2758–69. [PubMed: 19553649]

Malinen E, Rinttila T, Kajander K, Matto J, Kassinen A, Krogius L, Saarela M, Korpela R, Palva A (2005) Analysis of the fecal microbiota of irritable bowel syndrome patients and healthy controls with real-time PCR. Am J Gastroenterol 100(2):373–82. [PubMed: 15667495]

Mandrekar P, Bataller R, Tsukamoto H, Gao B (2016) Alcoholic hepatitis: Translational approaches to develop targeted therapies. Hepatology 64(4):1343–55. [PubMed: 26940353]

Mariotti V, Strazzabosco M, Fabris L, Calvisi DF (2018) Animal models of biliary injury and altered bile acid metabolism. Biochim Biophys Acta Mol Basis Dis 1864(4 Pt B):1254–1261. [PubMed: 28709963]

Nagy LE, Ding WX, Cresci G, Saikia P, Shah VH (2016) Linking Pathogenic Mechanisms of Alcoholic Liver Disease With Clinical Phenotypes. Gastroenterology 150(8):1756–68. [PubMed: 26919968]

Nanji AA, Mendenhall CL, French SW (1989) Beef fat prevents alcoholic liver disease in the rat. Alcohol Clin Exp Res 13(1):15–19. [PubMed: 2646971]

Odena G, Chen J, Lozano JJ, Altamirano J, Rodrigo-Torres D, Affo S, Morales-Ibanez O, Matsushita H, Zou J, Dumitru R, Caballeria J, Gines P, Arroyo V, You M, Rautou PE, Valla D, Crews F, Seki E, Sancho-Bru P, Bataller R (2016) LPS-TLR4 Pathway Mediates Ductular Cell Expansion in Alcoholic Hepatitis. Sci Rep 6:35610. [PubMed: 27752144]

Prado V, Caballeria J, Vargas V, Bataller R, Altamirano J (2016) Alcoholic hepatitis: How far are we and where are we going? Ann Hepatol 15(4):463–73. [PubMed: 27236145]

Rehm J, Imtiaz S (2016) A narrative review of alcohol consumption as a risk factor for global burden of disease. Subst Abuse Treat Prev Policy 11(1):37. [PubMed: 27793173]

Ritchie ME, Phipson B, Wu D, Hu Y, Law CW, Shi W, Smyth GK (2015) limma powers differential expression analyses for RNA-sequencing and microarray studies. Nucleic Acids Res 43(7):e47. [PubMed: 25605792]

Rusyn I, Bataller R (2013) Alcohol and toxicity. J Hepatol 59(2):387–8. [PubMed: 23391479]

Sancho-Bru P, Altamirano J, Rodrigo-Torres D, Coll M, Millan C, Jose Lozano J, Miquel R, Arroyo V, Caballeria J, Gines P, Bataller R (2012) Liver progenitor cell markers correlate with liver damage and predict short-term mortality in patients with alcoholic hepatitis. Hepatology 55(6):1931–1941. [PubMed: 22278680]

Seitz HK, Bataller R, Cortez-Pinto H, Gao B, Gual A, Lackner C, Mathurin P, Mueller S, Szabo G, Tsukamoto H (2018) Alcoholic liver disease. Nat Rev Dis Primers 4(1):16. [PubMed: 30115921]

Seki E, Schwabe RF (2015) Hepatic inflammation and fibrosis: functional links and key pathways. Hepatology 61(3):1066–79. [PubMed: 25066777]

Subramanian A, Kuehn H, Gould J, Tamayo P, Mesirov JP (2007) GSEA-P: a desktop application for Gene Set Enrichment Analysis. Bioinformatics 23(23):3251–3. [PubMed: 17644558]

Sun J, Fu J, Li L, Chen C, Wang H, Hou Y, Xu Y, Pi J (2018) Nrf2 in alcoholic liver disease. Toxicol Appl Pharmacol 357:62–69. [PubMed: 30165058]

Szabo G, Bala S (2010) Alcoholic liver disease and the gut-liver axis. World J Gastroenterol 16(11): 1321–9. [PubMed: 20238398]

Szabo G, Kamath PS, Shah VH, Thursz M, Mathurin P, Meeting E-AJ (2019) Alcohol-Related Liver Disease: Areas of Consensus, Unmet Needs and Opportunities for Further Study. Hepatology 69(5):2271–2283. [PubMed: 30645002]

Thompson JA, Reitz RC (1978) Effects of ethanol ingestion and dietary fat levels on mitochondrial lipids in male and female rats. Lipids 13(8):540–550. [PubMed: 703531]

Author Manuscript Author Manuscript Author Manuscript Author Manuscript

Tsukamoto H (2015) Metabolic reprogramming and cell fate regulation in alcoholic liver disease. Pancreatology 15(4 Suppl):S61–5. [PubMed: 25800177]

Ueno A, Lazaro R, Wang PY, Higashiyama R, Machida K, Tsukamoto H (2012) Mouse intragastric infusion (iG) model. Nat Protoc 7(4):771–81. [PubMed: 22461066]

Varemo L, Nielsen J, Nookaew I (2013) Enriching the gene set analysis of genome-wide data by incorporating directionality of gene expression and combining statistical hypotheses and methods. Nucleic Acids Res 41(8):4378–91. [PubMed: 23444143]

Wang L, Fouts DE, Starkel P, Hartmann P, Chen P, Llorente C, DePew J, Moncera K, Ho SB, Brenner DA, Hooper LV, Schnabl B (2016) Intestinal REG3 Lectins Protect against Alcoholic Steatohepatitis by Reducing Mucosa-Associated Microbiota and Preventing Bacterial Translocation. Cell Host Microbe 19(2):227–39. [PubMed: 26867181]

Zhou R, Fan X, Schnabl B (2019) Role of the intestinal microbiome in liver fibrosis development and new treatment strategies. Transl Res 209:22–38. [PubMed: 30853445]

Author Manuscript Author Manuscript Author Manuscript Author Manuscript

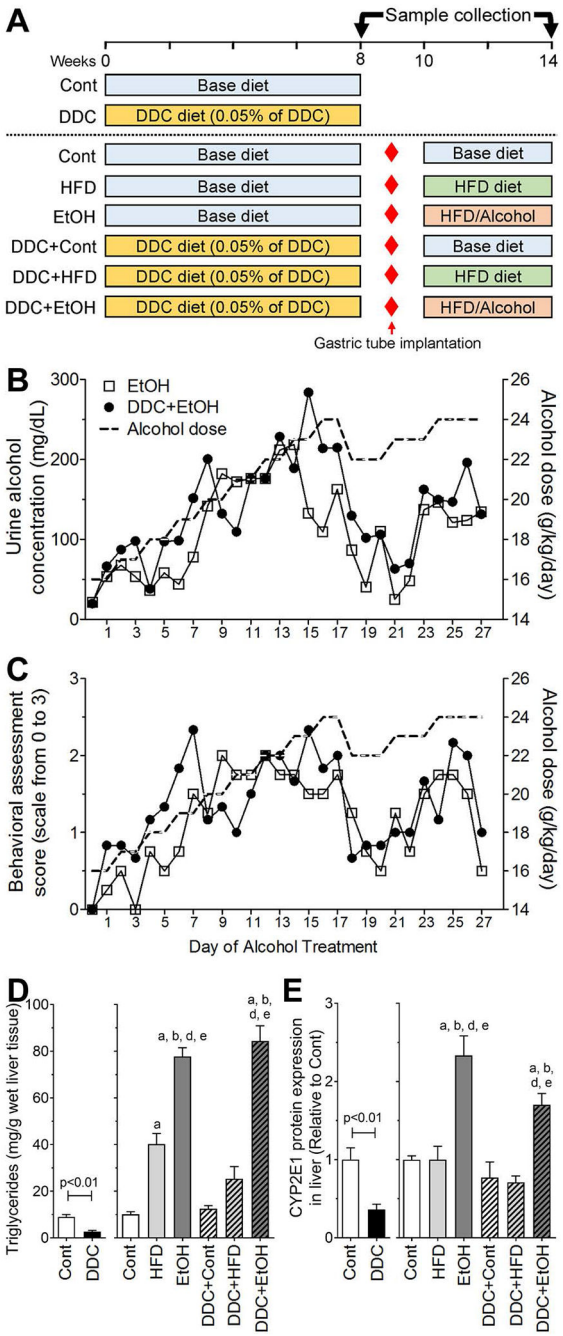

Figure 1.

(A) Overall study design. Treatment details for each group are detailed in Methods. (B) Daily average urine alcohol concentrations, and (C) behavioral scores in mice treated with control diets and/or DDC and fed alcohol or high-fat diet intragastrically. (C) Liver triglyceride levels. (D) Liver protein levels of CYP2E1. Data in C and D are presented as mean±SEM. T-test comparison p-value is shown for the 8 wk groups. Asterisks denote statistical significance (ANOVA followed by Tukey's multiple comparison test) as follows:

[a], p<0.05, compared with Cont group; [b], p<0.05, compared with HFD group; [d], p<0.05, compared with DDC+Cont group; [e], p<0.05, compared with DDC+HFD group.

Author Manuscript Author Manuscript Author Manuscript Author Manuscript

Author Manuscript Author Manuscript Author Manuscript Author Manuscript

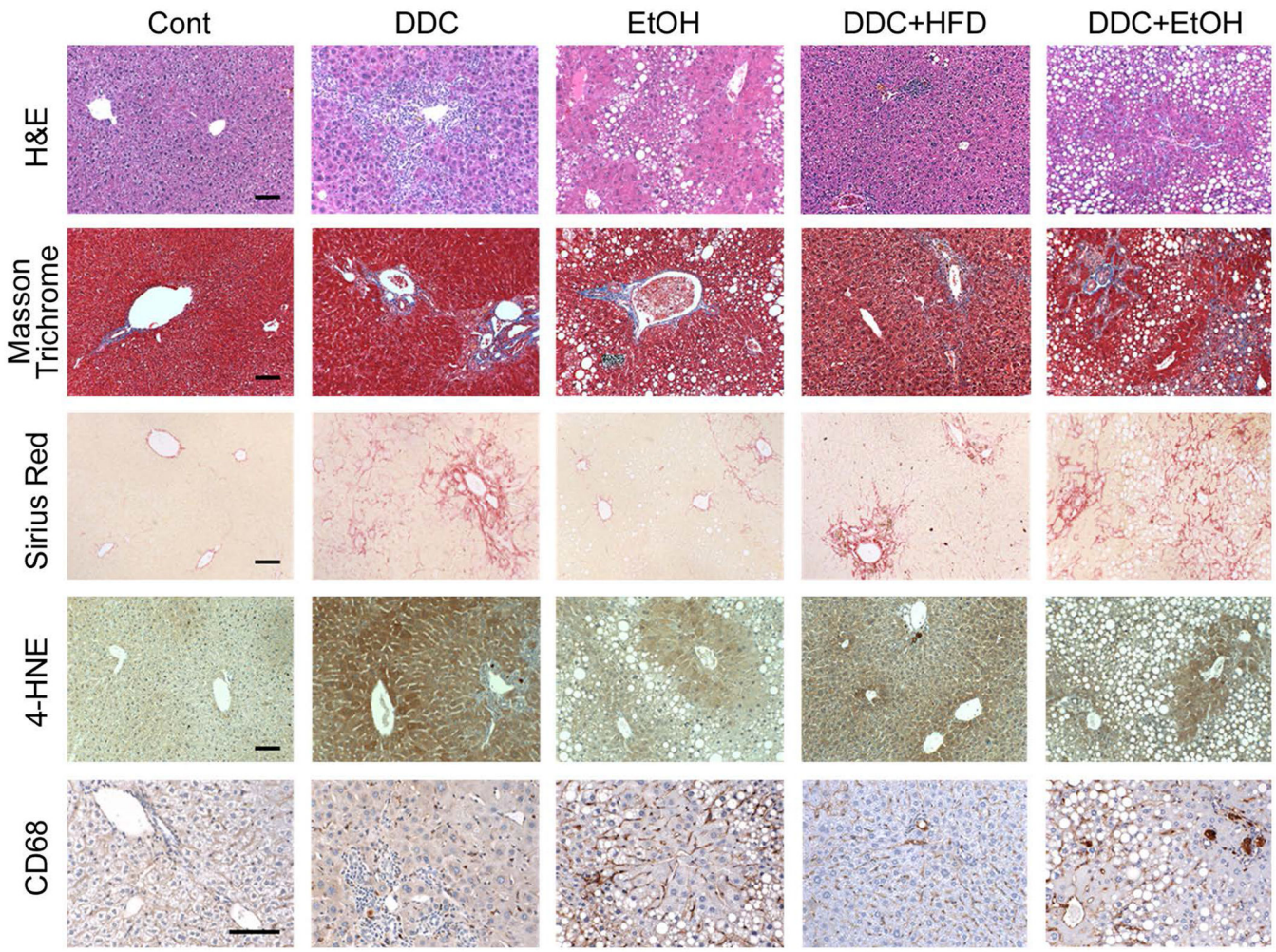

Figure 2.

Representative photomicrographs of liver sections from Cont, DDC, EtOH, DDC+HFD, and DDC+EtOH groups. Images are stained with hematoxylin and eosin (H&E), Masson trichrome or Sirius red stains, or were subject to immunohistochemical staining for 4-hydroxynonenal (4-HNE) or CD68 as detailed in Methods. Original magnification 100× for all phenotypes except for CD68 where magnification is 200×. Quantitative image analysis is presented in Figure 3.

Author Manuscript Author Manuscript Author Manuscript Author Manuscript

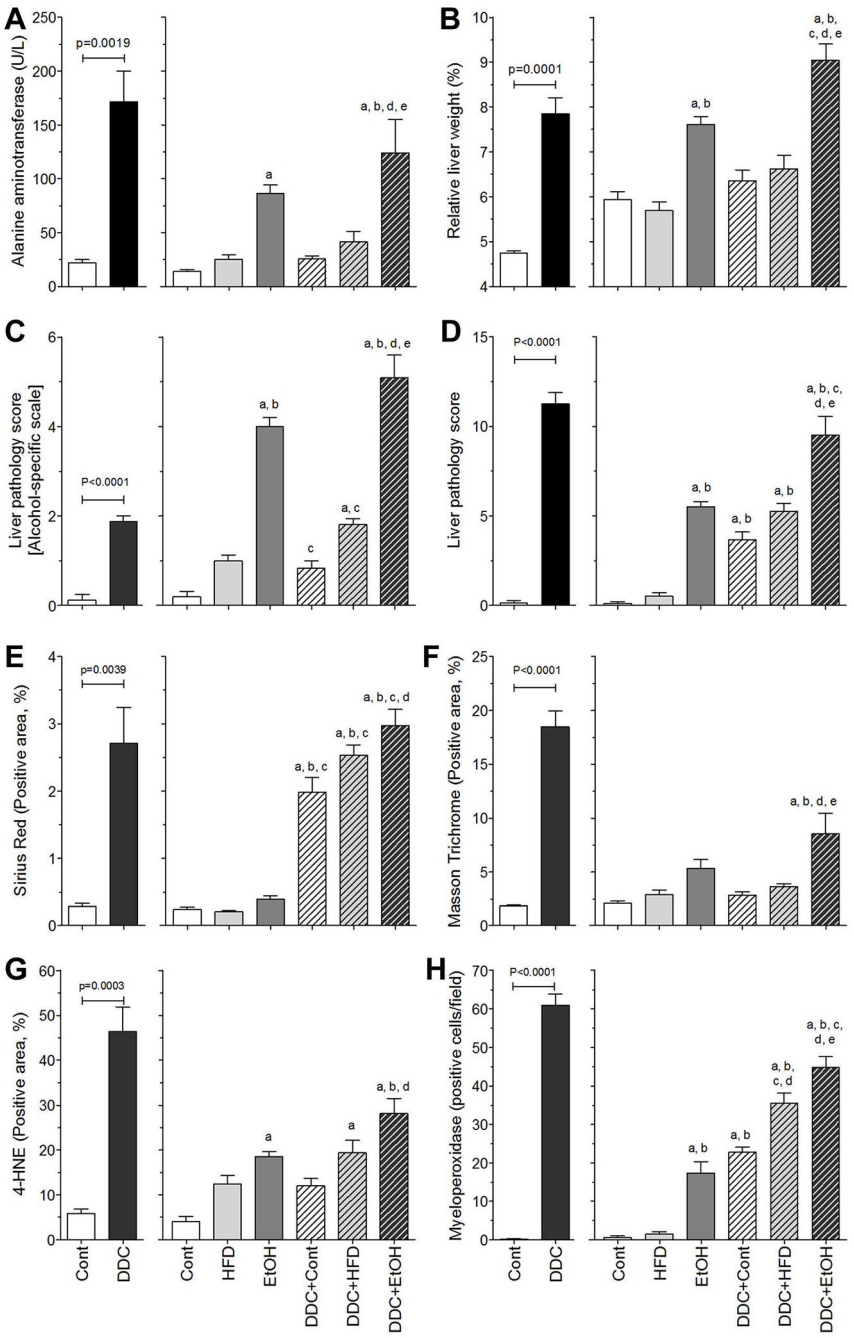

Figure 3.

Quantitative analysis of liver injury phenotypes. Shown are (A) serum ALT, (B) relative liver weight, (C-D) liver pathology scores, (E) Sirius red positive area, (F) Masson trichrome positive area, (G) 4-HNE positive area, and (H) myeloperoxidase positive area. All data are presented as mean±SEM. T-test comparison p-value is shown for the 8 wk groups. Asterisks denote statistical significance (ANOVA followed by Tukey's multiple comparison test) as follows: [a], $p<0.05$, compared to Cont group; [b], $p<0.05$, compared to HFD group; [c], $p<0.05$,

compared to EtOH group; [d], $p<0.05$, compared to DDC+Cont group; [e], $p<0.05$, compared to DDC+HFD group.

Author Manuscript Author Manuscript Author Manuscript Author Manuscript

Author Manuscript Author Manuscript Author Manuscript Author Manuscript

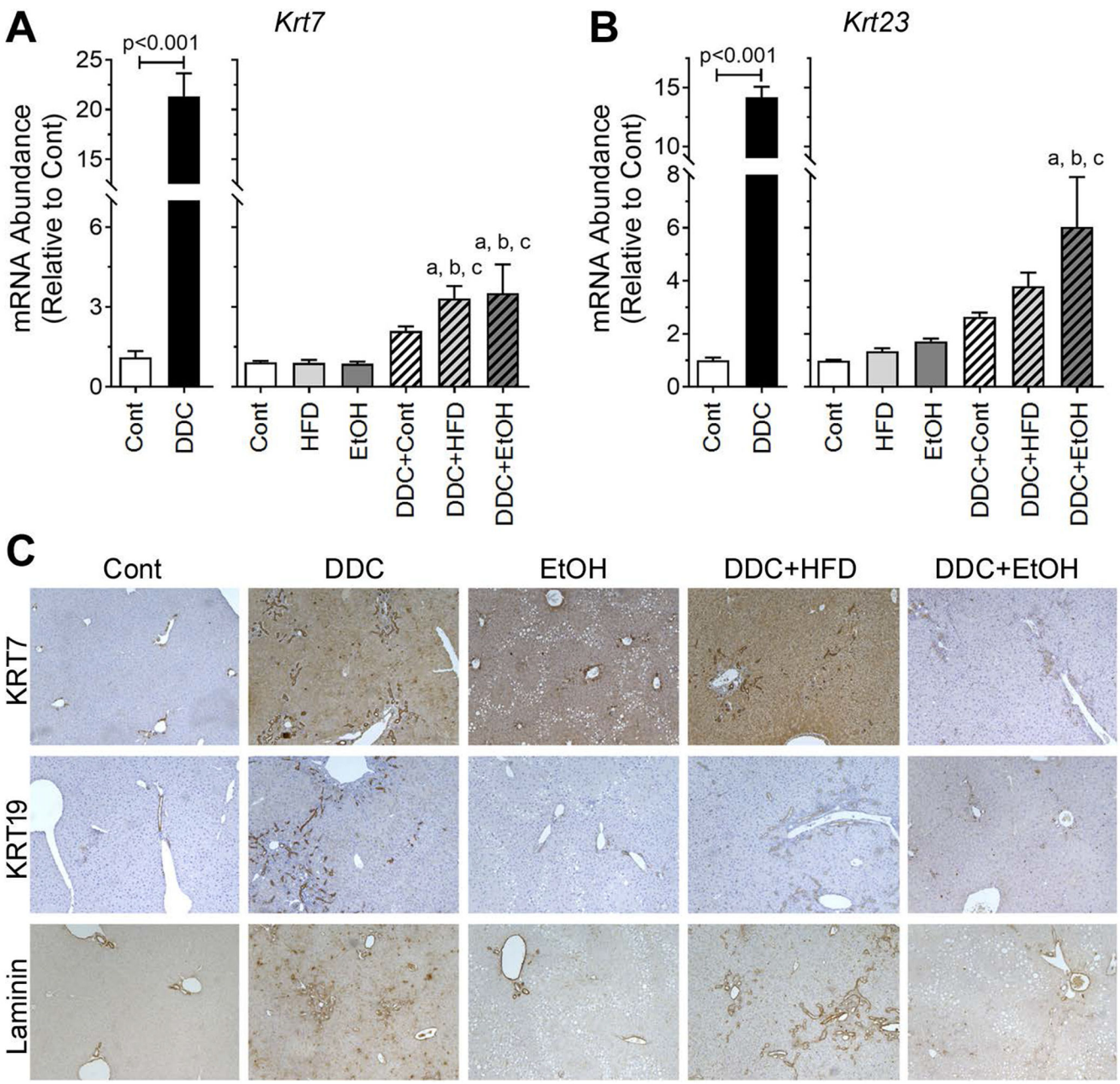

Figure 4.

Markers of ductular reaction. Expression of cytokeratins *Krt7* (A) and *Krt23* (B) in livers of mice in different treatment groups. All data are presented as mean±SEM. T-test comparison p-value is shown for the 8 wk groups. Asterisks denote statistical significance (ANOVA followed by Tukey's multiple comparison test) as follows: [a], $p<0.05$, compared to Cont group; [b], $p<0.05$, compared to HFD group; [c], $p<0.05$, compared to EtOH group. (C) Representative images of immunohistocemical staining of liver samples with antibodies against KRT7, KRT19 and laminin. Original magnification 100× for all phenotypes except for CD68 where magnification is 200×.

Author Manuscript Author Manuscript Author Manuscript Author Manuscript

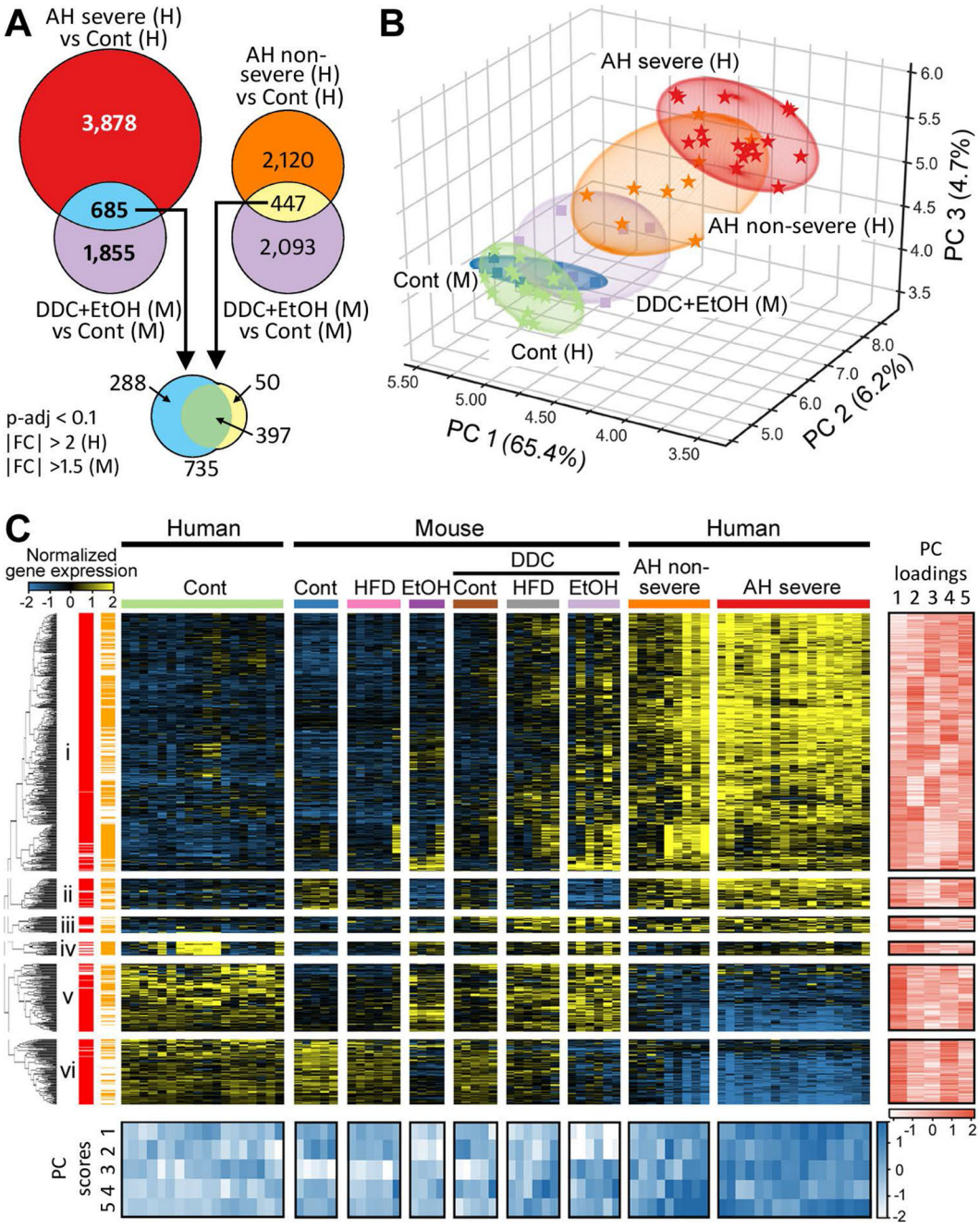

Figure 5.

Gene expression analysis of liver transcriptomes in mouse and human alcohol-induced liver disease. (A) Venn diagrams showing the overlap between significantly differentially expressed transcripts in human (H) and mouse (M) livers. Groups for which comparisons are displayed are indicated in the figure. Fold-change criteria are also indicated. (B) A principal components analysis based on gene expression data showing the similarity of transcriptional effects in the individual samples for groups indicated in the figure. (C) A heat map showing the relative expression of the 735 transcripts identified as commonly affected in both human

Author Manuscript Author Manuscript Author Manuscript Author Manuscript

and mouse alcohol- and fibrosis-associated disease. Transcripts were clustered (see dendrogram of the left hand side) and samples arranged into experimental groups (see labels along the top of the heat map). Red horizontal lines indicate transcripts affected in human samples, while orange ones show transcripts significantly affected in the mouse samples. Six clusters are separated for clarity of the visualization. Principal component scores for each transcript and sample, corresponding to the analysis shown in panel B, are shown for five top principal components.

Author Manuscript Author Manuscript Author Manuscript Author Manuscript

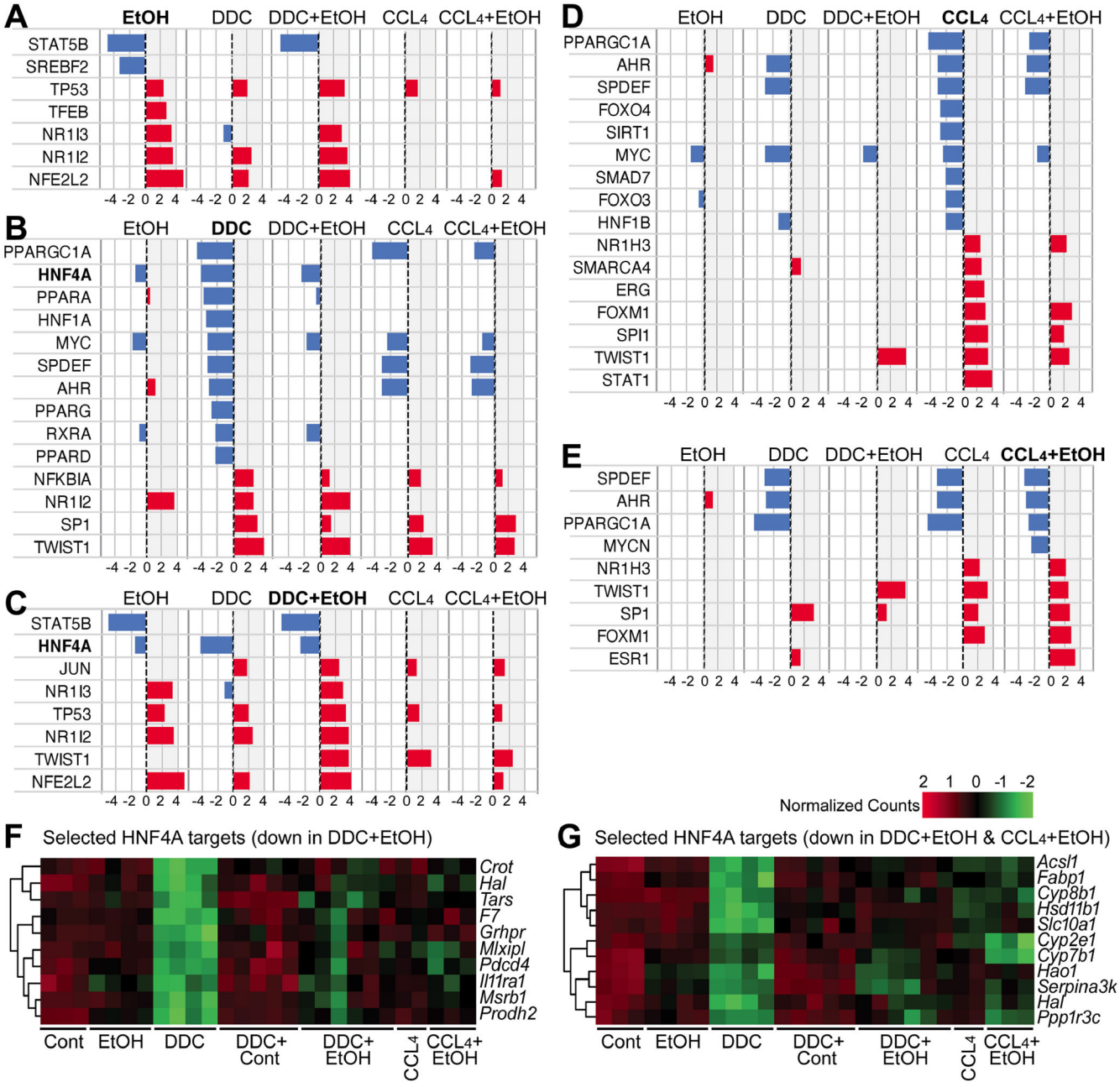

Figure 6.

Predicted transcription factor activity in the DDC-model and its comparison with CCl_4-model mice. Biased Z-Scores were obtained from the RNA-sequencing differential expression analysis comparing control mice with mice treated with only alcohol, DDC with our without alcohol or CCl_4 with or without alcohol. Results of Upstream Regulators analysis (see Methods) referring to the families “transcription regulator” and “ligand-dependent nuclear factor” are summarized. Results of predicted activation of transcriptional regulators are shown ordered by z-scores in EtOH-only group (A), DDC group (B), DDC +EtOH group (C), CCl_4 group (D), and CCl_4+EtOH group (E). Downregulation is shown by

Author Manuscript Author Manuscript Author Manuscript Author Manuscript

negative z-scores (blue) and induction by positive z-scores (red). All transcriptomic signatures had a Z-Score >+2 or <−2 and a p-value of overlap less than 10^{-4}. (F and G) Gene expression of selected targets of HNF4A transcription factor are shown. Genes that were significantly downregulated in DDC+EtOH group (F), or in both DDC+EtOH and CCL_4+EtOH groups, are shown separately. Gene expression was row-normalized and log2-transformed (see the color bar for relative expression).

Author Manuscript Author Manuscript Author Manuscript Author Manuscript

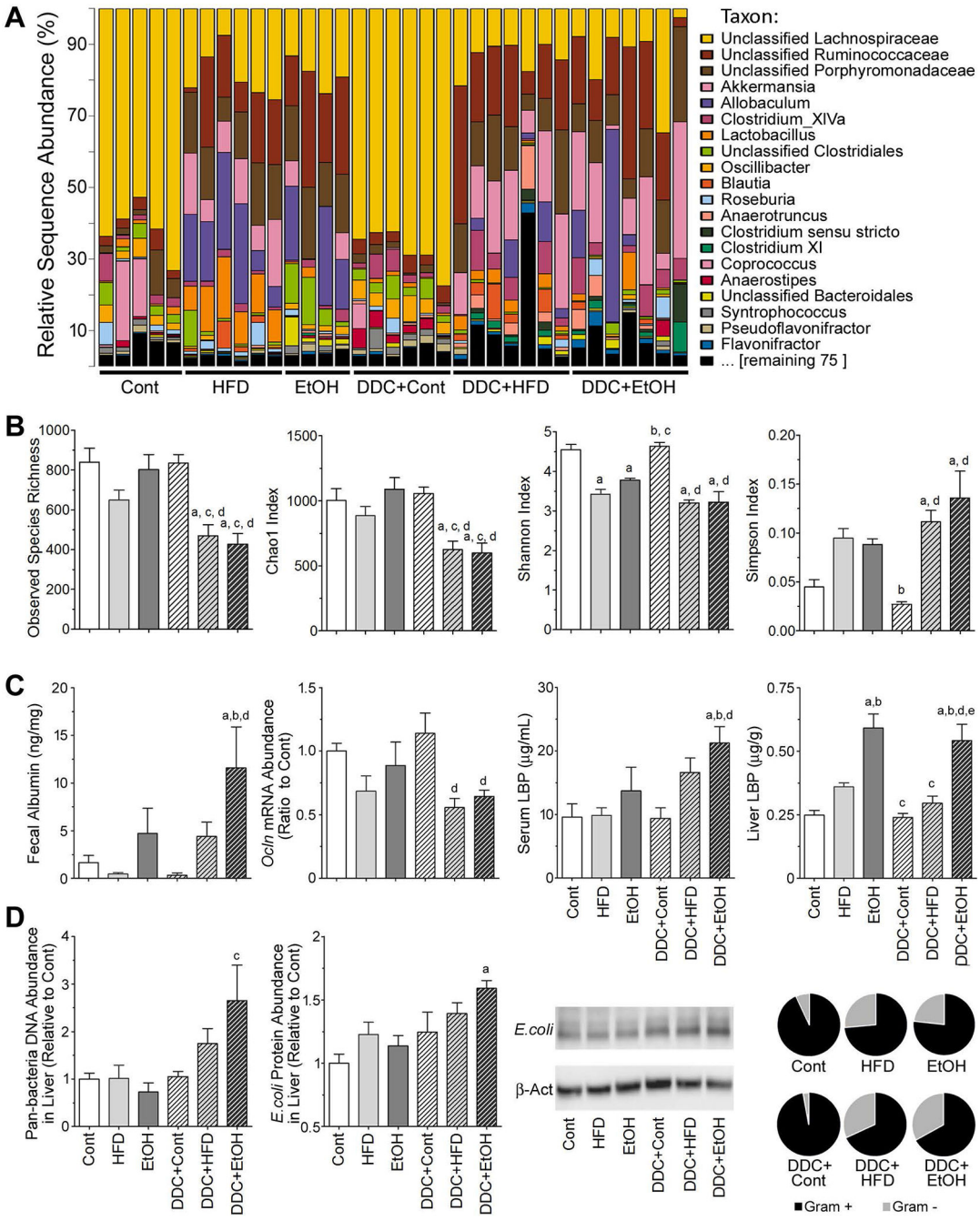

Figure 7.

Microbiome and bacterial translocation analyses. (A) 16S rRNA sequencing of fecal samples. The graph demonstrates the relative abundance of sequence reads in each genus and sample. Bacteria taxa legend is shown in the right panel. (B) Bacterial diversity (Shannon-Index and Simpson-Index) and richness (Chao-Richness) as calculated from microbiome analyses. (C) Gut permeability parameters fecal albumin, expression of *Ocln* mRNA in the gut, and presence of the lipopolysaccharide binding protein in serum and liver samples. (D) Bacterial translocation markers. Quantitative analysis of pan-bacteria DNA and

Author Manuscript Author Manuscript Author Manuscript Author Manuscript

E. coli protein in liver, and relative abundance of Gram+ (black) vs Gram– (gray) bacteria. In panels B-D, data are presented as mean±SEM. Asterisks denote statistical significance (ANOVA followed by Tukey's multiple comparison test) as follows: [a], $p<0.05$, compared to Cont group; [b], $p<0.05$, compared to HFD group; [c], $p<0.05$, compared to EtOH group; [d], $p<0.05$, compared to DDC+Cont group; [e], $p<0.05$, compared to DDC+HFD group.

Author Manuscript

Author Manuscript

Author Manuscript

Author Manuscript

Table 1.

Pathway enrichment analysis for the clusters of genes identified in Figure 5C.

	Transcript count	Percent enrichment	Fold enrichment	p-value (adjusted)**
Genes UP in human AND mouse AH (cluster i*)				
GO:0030198~extracellular matrix organization	35	8.4	7.6	6.3E-17
GO:0030574~collagen catabolic process	16	3.8	10.7	7.3E-09
GO:0033627~cell adhesion mediated by integrin	6	1.4	17.1	3.5E-03
GO:0048146~positive regulation of fibroblast proliferation	9	2.1	7.1	6.3E-03
GO:0051301~cell division	22	5.3	2.7	1.2E-02
GO:0050919~negative chemotaxis	7	1.7	8.8	1.7E-02
Genes DOWN in Mouse AND Human AH (cluster vi)				
hsa03320:PPAR signaling pathway	7	6.6	9.4	2.8E-03
GO:0006695~cholesterol biosynthetic process	5	4.7	21.7	1.6E-02
hsa04610:Complement and coagulation cascades	6	5.7	7.8	1.5E-02
Genes DOWN in Mouse UP in Human AH (cluster ii)				
GO:0006366~transcription from RNA pol II promoter	7	29.2	10.0	3.3E-03
GO:0032496~response to lipopolysaccharide	4	16.7	17.8	5.7E-02
Genes UP in Mouse and DOWN in Human AH (cluster v)				
GO:0031090~organelle membrane	6	5.5	11.6	2.0E-02

*, Clusters correspond to those shown in Figure 5C.

**, Benjamini-Hochberg adjusted p-values are shown.